Hydantoin-Based Molecular Photoswitches

David Martínez-Lo´pez,† Meng-Long Yu,‡ Cristina García-Iriepa,†,§ Pedro J. Campos,† Luis Manuel Frutos,§ James A. Golen,‡ Sivappa Rasapalli,*,‡ and Diego Sampedro*,†

†Departamento de Química, Universidad de La Rioja, Centro de Investigacio´n en Síntesis Química (CISQ), Madre de Dios, 51, 26006 Logron˜o, Spain

‡Department of Chemistry and Biochemistry, University of Massachusetts Dartmouth, North Darmouth 02747, United States

§Departamento de Química Analítica, Química Física e Ingeniería Química, Universidad de Alcala´, Alcala´de Henares, 28871 Madrid, Spain

Abstract:

A new family of molecular photoswitches based on arylidenehydantoins is described together with their synthesis and photochemical and photophysical studies. A series of hydantoin derivatives have been prepared as single isomers using simple and versatile chemistry in good yields. Our studies show that the photostationary states of these compounds can be easily controlled by means of external factors, such as the light source or filters. Moreover, the detailed investigations proved that these switches are efficient (i.e., they make efficient use of the light energy, are high fatigue resistant, and are very photostable). In some cases, the switches can be completely turned on/off, a desirable feature for specific applications. A series of theoretical calculations have also been carried out to understand the photoisomerization mechanism at the molecular level.

Introduction

In recent years, molecular switches and motors (1, 2) have been used in very different applications with great success. Specifically, photoactive molecular switches have been used to control diverse properties from the shape of crystals (3) to protein engineering, (4) activity of biological systems, (5) and orientation in liquid-crystalline polymers. (6) Modifying the structure of the switch and thereby the properties of complex systems by light as the external stimulus has some advantages: (1) (1) selected wavelengths can be used to minimize the damaging effect of light in the system, (2) a high degree of spatial and temporal resolution can be obtained, and (3) no waste products are obtained after photon absorption. In spite of the increasing number of promising applications for photoswitches, most of the compounds employed to photocontrol the properties of complex systems share a common set of basic chemical properties. The available molecular photoswitches can be classified into two main classes depending on the photochemical process that allows the switch between the two isomeric forms. Type 1 compounds can photoisomerize between closed and open forms. Among this type of photoswitches, the dimethyldihydropyrene (DHP)/cyclophanediene (CPD) system, (7-10) diarylethenes, (11-13) and spiropyranes (14-17) have been developed. Type II compounds undergo isomerization of a double bond as in *E/Z* photochemical switches. Of the several families of *E/Z* photochemical switches, azobenzenes (18-20) have been used extensively due to their stability, adequate photophysical properties, and ease of synthesis and derivatization. Furthermore, overcrowded alkenes (21) have been

applied as photoswitches to control diverse properties but also as frameworks in the preparation of molecular motors. (22) Several other switches have been reported, (23) including retinal-based switches, (24-29) green fluorescence protein (GFP) analogues, (30, 31) and hemithioindigos. (32-38) Although numerous efforts have been made to generalize the concept of a molecular photoswitch at the theoretical level, (39) preparation and photochemical studies of new families of switches seem critical for enabling more complex and specific applications. To this end, we have been intrigued by the possibility of developing a new family of photoswitches based on 5-arylidenehydantoins.

5-Arylidenehydantoins (5-AHTs) belong to a novel family of (GFP) analogues, where the imidazoline unit is replaced by an imidazolinone moiety. (23) The first synthesis of 5-AHT, from the reaction of phenylpropiolic acid with urea, was reported in 1899. (40) Some years later, Wheeler and Hoffman described a more effective method to prepare 5-AHT from the condensation of hydantoin and benzaldehyde in acidic solution. (41) Applications of 5-AHTs are mainly focused on their biological activities. To date, multiple functions, such as anticancer, antibiotic, and antagonistic properties, have been reported. (42) However, there are only scant reports about the study of their photochemical properties. In this respect, it has been demonstrated (43) that 5-AHTs function as excellent UV absorbents in the cosmetics industry. On the basis of the structural similarity of 5-AHTs with the GFP-like molecular photoswitches previously reported, (44) the capability of *Z*/*E* photoisomerization, (45-47) and their superb thermal and photochemical stability, we decided to explore their behavior as molecular photoswitches. Accordingly, we have carried out detailed investigations and herein report the synthesis, photochemistry, and theoretical study of a library of molecular photoswitches based on the 5-arylidenehydantoin structure.

Scheme 1

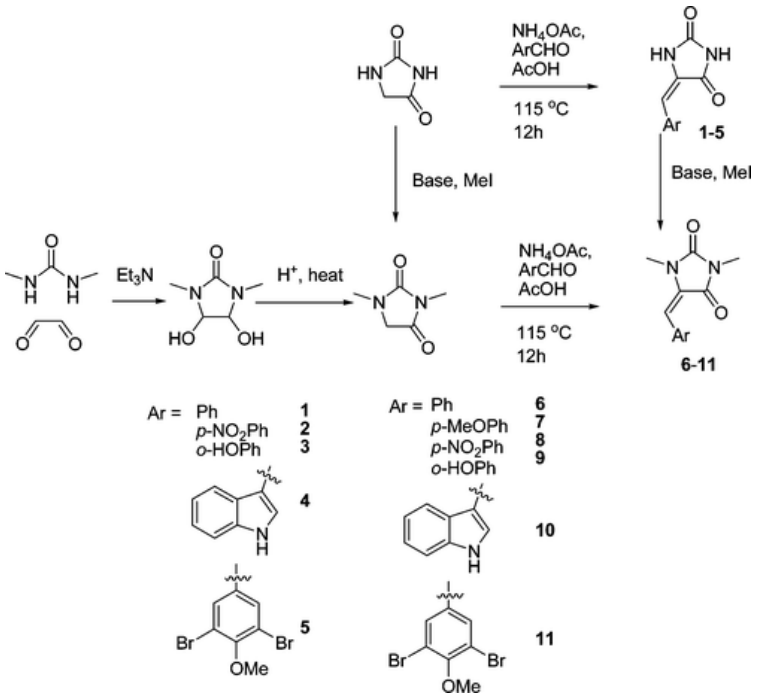

Scheme 1. Synthesis of Compounds **1**–**11**

2 Results and Discussion

This new series of molecular photoswitches was synthesized according to Scheme 1. Thus, 5-arylidenehydantoin derivatives **1**–**5** were synthesized from the condensation of hydantoin and different aromatic aldehydes in an acetic acid/ammonium acetate mixture in good yields (70–80%, see Supporting Information for synthetic details) according to a previously reported method. (48) The disubstituted 1,3-dimethyl-5-arylidenehydantoins **6**–**11** were obtained in two different ways. In the first method, 5-arylidenehydatoins that were previously synthesized from aldehydes and hydantoin condensation as described above were subjected to bis-methylation with excess methyl iodide to produce the 1,3-dimethyl-5-arylidenehydantoin series. However, this method was limitated with respect to purification and the presence of other potential nucleophilic functionalities. Thus, we resorted to an alternative method to solve this problem by accessing the dialkylated precursor (i.e., 1,3-dimethylhydantoin obtained via either de novo synthesis or through bis-methylation of hydantoin. Thus, treatment of glyoxal with *N, N*'-dimethylurea followed by pinacol rearrangement delivered the clean formation of 1,3-dimethylhydantoin. Condensation of this compound with various aldehydes afforded the 1,3-dimethyl-5-arylidenehydantoins as final products. Under both reaction conditions, the *E* isomer was found to be the only isomer. In all case, the *Z* isomer was not detected by NMR. The configuration of the obtained products was in turn confirmed by X-ray diffraction data for **7** (Figure 1).

Figure 1

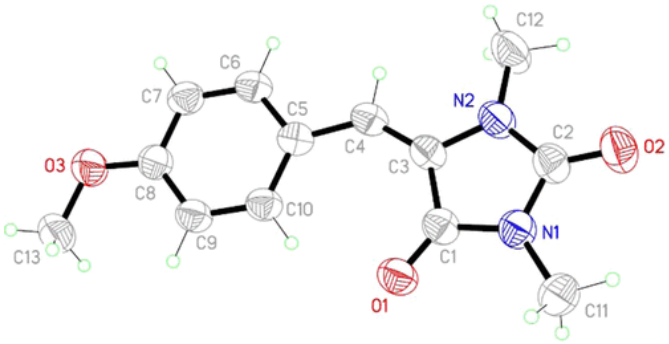

Figure 1. Solid state structure of ***E*-7** with thermal ellipsoids shown at 50% probability.

All of the hydantoin-based compounds synthesized share a typical UV absorption spectrum as exemplified in Figure 2 by the spectrum of **7** in CH_2Cl_2/MeOH (1:1). In all of the cases, a strong absorption band between 320 and 370 nm was found for **1**–**11** (see Table 1). This is relevant as low-energy wavelengths could be used to promote the photoisomerization, which in turn confers a wider applicability to these switches. Furthermore, the solvent effect was investigated by recording the UV spectra in acetonitrile, chloroform, and DMSO. No significant changes were detected in the spectra for the tested solvents. The effect of dimethylation of the hydantoin moiety has a minor effect on the absorption spectra of these compounds. A small shift of 10–15 nm was found when comparing 5-

arylidenehydantoins **1**–**5** with their equivalent 1,3-dimethyl-5-arylidenehydantoins **6**–**11**. However, the two series of compounds show different solubility features, as **1**–**5** are only soluble in CH_2Cl_2/MeOH mixtures and DMSO whereas **6**–**11** are very soluble in common organic solvents. Thus, different experimental conditions are available for these switches while the absorption properties remain similar.

Figure 2

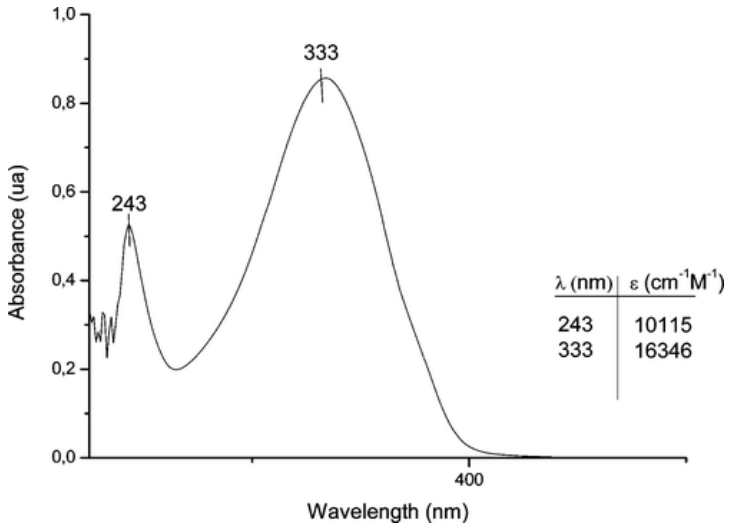

Figure 2. UV–vis spectrum of **7**.

Irradiation of compounds **1**–**11** was performed with a 400 W medium-pressure Hg lamp through a Pyrex filter (to avoid light with wavelengths below 290 nm) in an immersion well or in a Pyrex NMR tube. The progress of the reaction was easily monitored by ^{1}H NMR and TLC as the *Z* and *E* isomers for every compound show clearly different chemical shifts (especially the vinyl hydrogen) and R_f values. For instance, the vinyl hydrogen of **1** appears in ^{1}H NMR as two distinct singlets at 6.41 (***E*-1**) and 6.32 ppm (***Z*-1**, see Supporting Information). In the case of **5**, these two signals appear at 5.59 (***E*-5**) and 6.33 ppm (***Z*-5**). Thus, photoisomerization could be easily and quantitatively followed by NMR. Irradiation was maintained until the photostationary state (PSS) was reached. Typically, this required ~45 min in a Pyrex tube. The composition of the PSS under these conditions for compounds **1**–**11** is shown in Table 1.

Interestingly, no decomposition was observed by NMR in the course of the photoisomerization even after several hours of continued irradiation once the PSS was reached. This is relevant as potential applications of these switches that require long periods of irradiation could be envisaged. Thus, photostability is a valuable feature for any photoswitch. We have further probed the stability of compounds **1**–**11** in two different ways. First, all the compounds were subjected to further irradiation for at least 4 h after the PSS was reached (~45 min). In none of the cases was decomposition observed by NMR. It should be noted that during this time both isomers are continuously absorbing and reacting in a dynamic equilibrium. As a second measure of photostability and capability for performing

several cycles without decomposition, several photoisomerization cycles were performed for compounds **2** and **7** as representative examples (Figure 3). For instance, a solution of ***E*-7** was irradiated using light of alternating 375 and 300 nm wavelengths, and the isomerization was followed by the absorbance at 333 nm (maximum absorption wavelength for ***E*-7**). Both isomers could be interconverted for several cycles without apparent decomposition. Therefore, those two experiments indicate the high photostability and fatigue resistance of these switches, which is a prerequisite for practical applications.

Table 1. Absorption Maximum and Photostationary State (PSS) for 1–11 at Different Irradiation Wavelengths in 1:1 CH_2Cl_2/MeOH

compound	λ_{max}[a]	PSS (*E*:*Z*)[b]	PSS (*E*:*Z*)[c]
1	317	100:0[d]	95:5
2	353	64:36	53:47
3	340	86:14	48:52
4	367	89:11	22:78
5	321	0:100	19:81
6	309	100:0[d]	
7	333	5:95	35:65
8	339	69:31	
9	326	88:12	
10	373	45:55	
11	316	100:0[d]	

[a]Value in nm for *E* isomer.
[b]Using a Pyrex-filtered medium-pressure Hg lamp.
[c]Using a photoreactor at 350 nm.
[d]Photoisomerization takes place in quartz, see text.

Figure 3

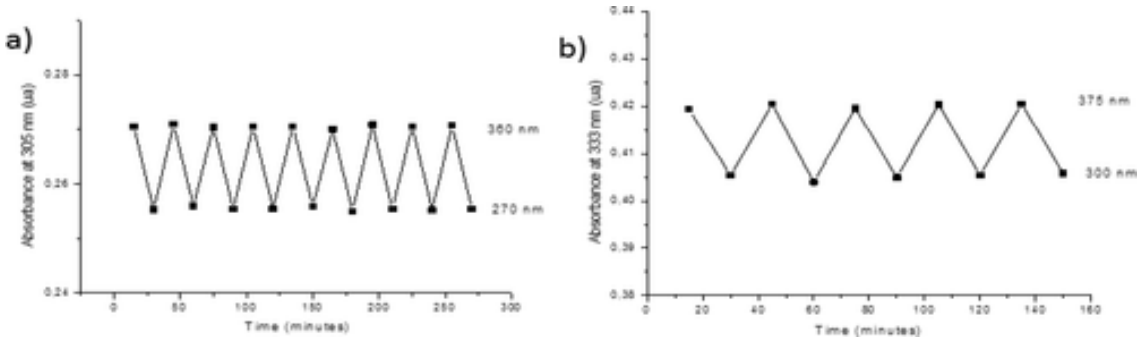

Figure 3. Photoisomerization cycles for (a) **2** and (b) **7**.

In addition, the photoisomerization kinetics were studied for ***E*-7** using ^{1}H NMR to determine the relative concentrations at short irradiation time intervals (Figure 4). From the first points, when the composition of the mixture is mainly the *E* isomer and absorption of the *Z* isomer is minimized, a kinetic constant of 2.57 s^{-1} was obtained. Thus, we concluded that under these conditions a fast photoisomerization takes place.

Figure 4

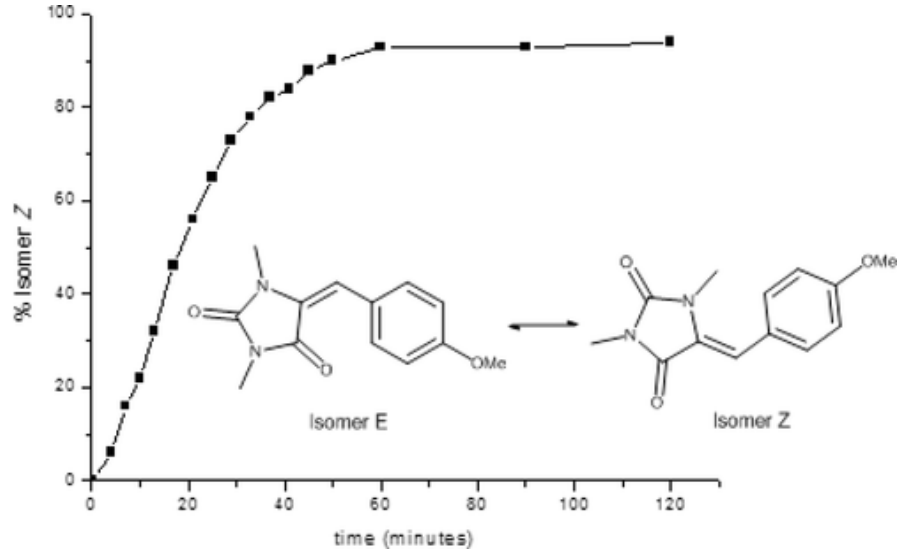

Figure 4. Composition of the mixture during irradiation of ***E*-7** at different time intervals.

As shown in Table 1, the PSS ratio is strongly dependent on the aryl substituent as different *E*:*Z* ratios were obtained. The composition of the PSS is affected by the relative absorption of the isomers, their relative stability, and the topology of the potential energy surfaces. In turn, all these factors could be different for every compound in Table 1. Also, the PSS depends on the quantum yields of the forward (*E* → *Z*) and backward reactions (*Z* → *E*). In turn, these quantum yields are affected by the relative absorption of both isomers and the shape of the potential energy surfaces. Thus, providing a general quantitative rationale of the PSS is a complex issue. However, some qualitative indications of the relevance of these factors could be obtained. As the relative absorption of the *E* and *Z* isomers is clearly dependent upon the irradiation source, a different PSS could be obtained for the switches under different irradiation conditions (see below). In this case, it is relevant to check which isomer absorbs light preferentially at a specific light source or wavelength. Also, the topology of the potential energy surface is relevant to determine the composition of the PSS. For these compounds, the decay to the ground state after excited state relaxation implies a geometry twisted ∼90° (see the computational paragraphs below). However, this torsion angle is expected to be affected by the electronic nature of the substituents as has been found for other *E*/*Z* photoswitches. (23) Complete exploration of the effect of substitution (in both the absorption spectrum and the potential energy surface topology) is beyond the scope of this paper. However, some conclusions can be derived from the analysis of Table 1. For instance, in most cases, the thermally stable isomer *E* is also the main isomer in the PSS when a Pyrex filter is used (see **2**–**4**, **8**–**9**, Table 1). This is probably due to the slightly stronger absorption of the *E* isomers under these irradiation conditions (see Supporting Information). A different situation was found for **1**, **6**, and **11**, as these compounds do not photoisomerize under the same conditions. However, for all three compounds, photoisomerization can take place by simply removing the filter and using a quartz-filtered light. In these cases, the

relative absorption of both isomers changes when the irradiation source is modified. Under these different conditions, the PSS is 79:21 for **1,** 61:39 for **6**, and 54:46 for **11**. Isolation of photoproduct ***Z*-1** by column chromatography allowed for recording of the UV spectrum (see Figure 5).

Figure 5

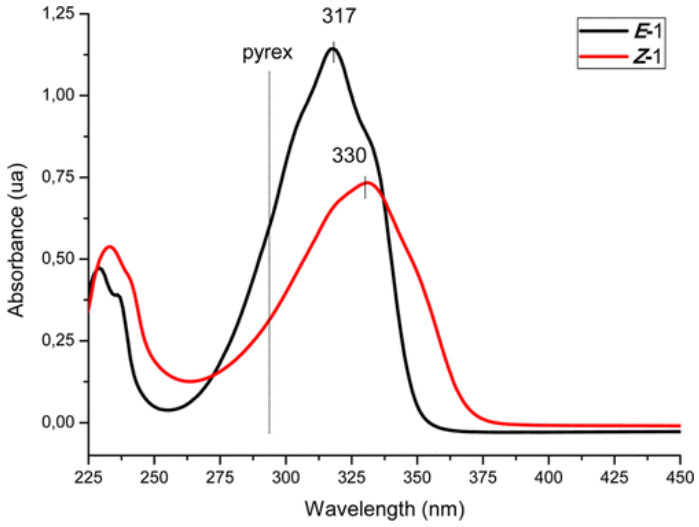

Figure 5. UV–vis spectrum of ***E*-1** and ***Z*-1**.

As can be seen, the photoisomer features a tail at longer wavelengths, causing higher absorption when a Pyrex filter is used. Thus, although photoisomerization can take place, the back reaction from the *Z* isomer to the thermally stable *E* isomer is faster under these conditions. However, when quartz-filtered light is used, the whole band of the *E* isomer is included in the absorption window, and the competitive back-reaction is not that effective, allowing for the observed PSS. We validated this effect by following the conversion of a pure ***E*-1** sample until the PSS was reached using ^{1}H NMR (Figure 6).

Figure 6

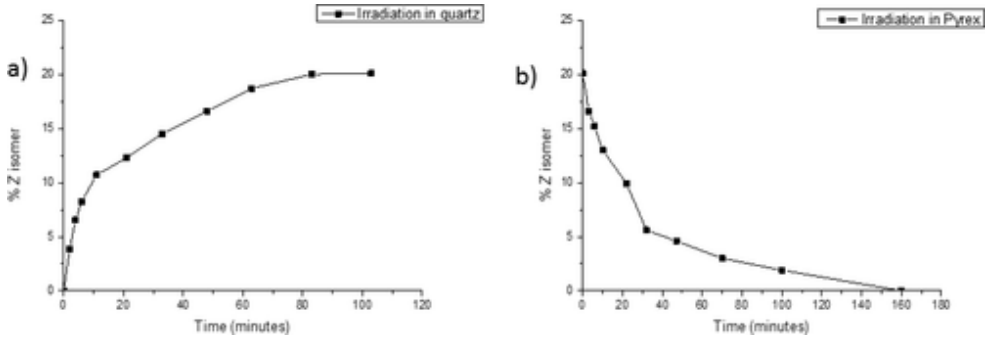

Figure 6. Composition of the mixture under irradiation of **1** using (a) quartz and (b) Pyrex filters.

As can be seen, using a quartz filter, the irradiation continuously induces photoisomerization of **1** until a mixture of isomers in a 79:21 ratio is reached

(Figure 6, a). Subsequent irradiation of the same solution through a Pyrex filter leads to the starting situation of pure *E*-isomer (Figure 6, b). Alternative irradiation of the same sample of **1** using Pyrex and quartz as filters during several cycles allowed for the formation of different mixtures with Pyrex and quartz with no observable decomposition (Figure 7). We anticipate that this stability allows the PSS to be easily altered by an external agent as does the use of different types of filters. In addition, this result proves the high fatigue resistance of the hydantoin-based switches under relatively long irradiation times even using a high-energy irradiation source. The same behavior was also found for **6** and **11**.

Figure 7

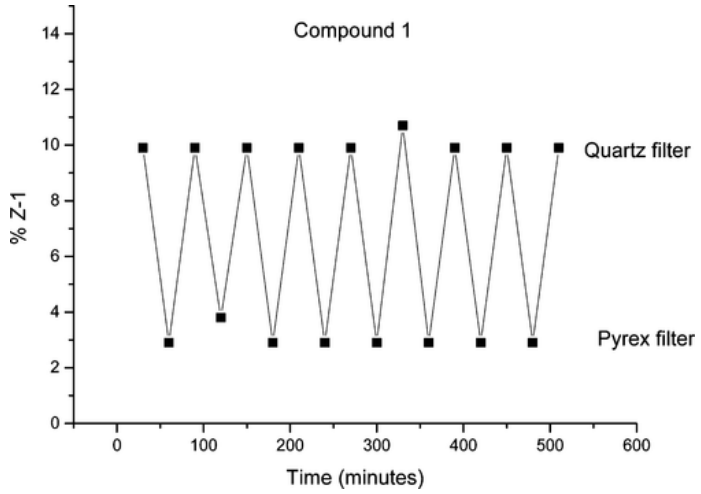

Figure 7. Photoisomerization cycles for **1**.

Some relevant results were also found for **5** and **7**. In these two cases, the *Z* isomer was not only the main product in the PSS, but it was obtained almost quantitatively. This implies that, starting from the pure ***E*-5** obtained directly from synthesis, only photoisomer ***Z*-5** was detected by NMR after irradiation. This excellent feature allows for a complete change in the switch position; that is, the switch can be completely changed from the *off* state to the *on* state. Although this is highly desirable for photoswitches, such a complete change is not at all common. In fact, most systems reported in the literature only allow for modification of the PSS but not a complete change in the switch state. (2)

To generalize the effect of the light source on the process, we also tested the photoisomerization using a photoreactor with emission centered at 350 nm (14 lamps × 8W/lamp). For this, we chose compounds **2**–**4**, as they showed neat absorptions in the 350 nm region (see Supporting Information, Figure S1), together with **1**, **5**, and **7** to check the generality of the effect. The results are shown in Table 1. For **2**–**4**, the use of this light source causes a different PSS enriched in the *Z* isomer (see Supporting Information, Figures S2–S4). Again, this fact attests additional practical flexibility of these systems, as the PSS can also be modified easily with an external agent.

Furthermore, the effect of monochromatic light in the photoisomerization process was studied. For this study, we chose **5** and **7**, as the *Z* isomer was found almost

exclusively in the PSS. The comparative UV spectra for the *E* and *Z* isomers of **5** and **7** are shown in Figures S5 and S6 in the Supporting Information. Regarding **5**, the thermal *E* isomer featured stronger absorption along the complete range of wavelengths. Thus, its irradiation would lead in all cases to the *Z* isomer as the main isomer in the PSS. However, in the case of **7**, both isomers showed slight displacement between their absorption maxima. Although small, this difference could be enough to displace the PSS. We tested this fact by irradiating at three different wavelengths, namely, 300, 333, and 375 nm. The results are shown in Table 2.

Table 2. Irradiation of 7 at Selected Wavelengths

λ (nm)	*E* isomer (%)	*Z* isomer (%)
300	78	22
333	55	45
375	25	75

Hence, it can be concluded that small variations in the irradiation wavelength lead to significant changes in the PSS. For **7** specifically, changing the irradiation wavelength from 300 to 375 nm may change the primary isomer in the PSS from the *E* to the Z isomer. This fact shows the enormous versatility of this new family of molecular switches that can be interchanged between both states with ease. To further clarify the effect of monochromatic light, we followed the irradiation of fresh samples of pure ***E*-7** using light of various wavelengths, namely, 300, 333, and 375 nm (Figure 8). As can be seen, the PSS is different for each wavelength, with 22%, 45%, and 75% of *Z* isomer, respectively (Table 2). Also, using light at 375 nm, the PSS (75% *Z* isomer) is reached faster than using light at 300 or 333 nm. It should be noted that the absorption at 333 nm is higher for both isomers (see Supporting Information, Figure S6). These facts can be explained by the relative absorption of both isomers at each wavelength. As both the forward ($E \rightarrow Z$) and reverse ($Z \rightarrow E$) reactions take place, the kinetics and the PSS are affected by the difference in absorption of both isomers. In this specific case, the absorption difference is bigger at 375 nm, which explains the reported results.

Figure 8

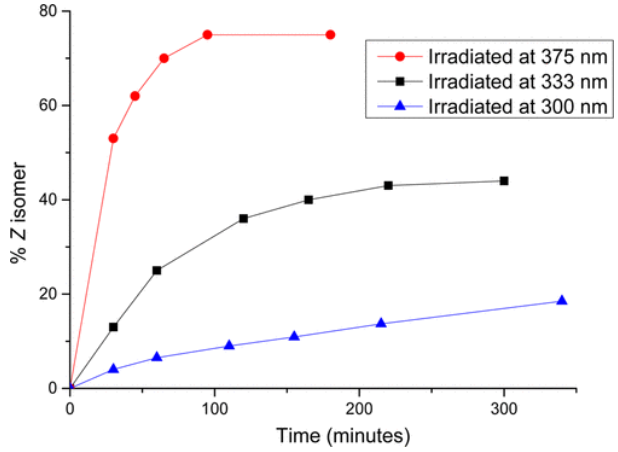

Figure 8. Composition of the mixture when irradiating ***E*-7** using monochromatic light.

With the feasibility of photoisomerization established, their relative efficiency relative to alternative deactivation pathways needed to be evaluated to determine the proficiency of these compounds as molecular photoswitches. A common competitive pathway with photoisomerization is fluorescence emission. Thus, we checked the luminescent properties of **2**, **7**, and **8** as representative examples (see Figure 9 and the Supporting Information, Figures S7 and S8).

Figure 9

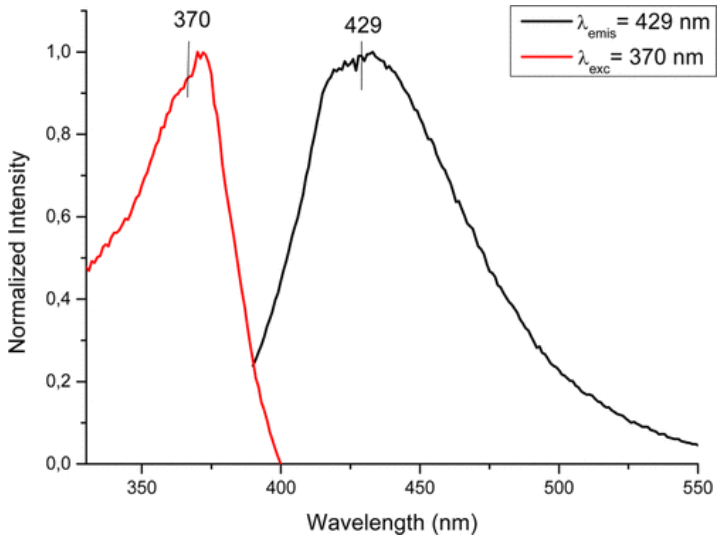

Figure 9. Excitation and emission spectra for **7**.

A similar emission pattern was found for **2**, **7**, and **8**, as a single emission band was found each of the cases. For **7**, the emission is located at 429 nm, whereas the band is centered at ~530 nm for **2** and **8**. A slightly bigger Stokes shift was found in the case of **8** (150 nm). However, in all cases, the emission quantum yield was below the apparatus threshold, which in our case allowed us to set an upper limit of Φ_{em} < 0.1%. (49) Thus, we proved that the radiative deactivation of the excited state is not a competitive pathway. To quantify the efficiency of the photoisomerization, we measured the reaction quantum yield for **3** and **7** as representative examples. Using *trans*–azobenzene as an actinometer (50) and measuring the conversion of the *E* to *Z* isomer at short times, we obtained a Φ of 15 ± 1% for irradiation at 334 nm for **3** and 16 ± 1% for **7**. Although these values are not as high as some recently reported, (44) they do confirm that this new family of compounds is quite efficient and promising.

Finally, the thermal reverse-reaction of the *Z* to *E* isomer was also measured for different compounds, as this could be relevant for some potential applications. Although thermal stability of the photogenerated isomer is usually desirable, for some applications, a fast thermal back-reaction is required. (51) Thus, we studied thermal isomerization of the *Z* isomer for **4**, **5**, and **7**. A slow back-reaction (1 week) was found for **4** at 70 °C but not for **5** or **7**. Increasing the temperature to 100 °C lead to faster isomerization of **4** and some degree of isomerization for **7** (22 days), whereas no back-reaction was found for **5.** In this case, slow thermal degradation was found by NMR upon heating at 120 °C (2 days). Thus, in general, these

compounds proved to be quite stable to the thermal back reaction. The different time scales found can be attributed to the electronic influence of the substituents on the aryl moiety that affect the transition structure of the isomerization.

To understand the photophysics and photochemistry of the reported photoswitches, a computational study using the MS-CASSCF//CASPT2 methodology (52, 53) was performed on **7** as a representative example (see the Supporting Information for computational details). First, the structures of the *E* and *Z* isomers were optimized in the ground state at the MP2/6-31G* level of theory (Figure 10). The *E* isomer minimum is planar, and the *Z* isomer is slightly twisted due to steric hindrance between the methyl and phenyl group. Indeed, the phenyl group is much more twisted (~47°, dihedral C5 C4 C3 C2) compared to the *E* isomer.

Figure 10

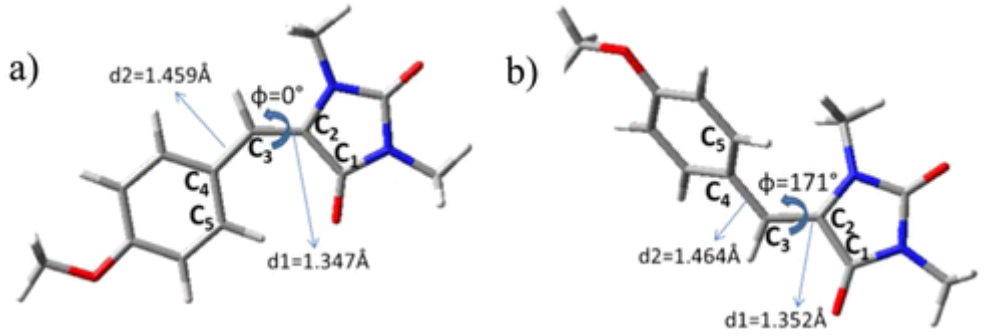

Figure 10. Structure of the ground state minima for the (a) *E* and (b) *Z* isomers of compound **7** (C1 C2 C3 C4 dihedral is defined as ϕ).

The absorption spectrum for both isomers and the photoisomerization mechanism of the *E* isomer (thermally stable) were calculated with the MS-CASPT2//SA-CASSCF methodology using a 6-31G* basis set. For the absorption spectra simulation, we chose six π orbitals (all π backbone), the corresponding π* orbitals, and two n orbitals (one of the nitrogen atom and the other of the carbonyl moiety closer to the chromophore). Then, the active space was reduced by removing those orbitals with almost 2.0 or 0.0 occupation numbers to calculate the minimum energy path, including 5 π orbitals, the corresponding π* orbitals, and one n orbital of the carbonyl moiety (see Supporting Information for complete details), obtaining the same energetics as in the large active space.

Both isomers exhibited similar absorption spectra as observed experimentally. The first excited state (S_1) is optically bright (see Table 3), whereas the second (S_2) and the third (S_3) excited states are dark states (see Table 3). The electronic transition nature of S_1 is described mainly by the excitation of one electron from the bonding π to the antibonding π* orbital of the central $C_2{=}C_3$ bond that is selective to photoisomerization (see Supporting Information, Figure S9). S_2 and S_4 are also described by excitation (single and double, respectively) from one bonding π to one antibonding π* orbital, whereas the $S_0 \rightarrow S_3$ electronic transition is due to monoexcitation from an n orbital to an antibonding π* orbital. The effect of the

solvent was modeled by applying the polarizable continuum model (PCM), obtaining similar results as those found for the gas phase (Table 3).

Table 3. Experimental (Chloroform), CASPT2 Vertical Transitions Energies (Gas Phase and in Chloroform), Electronic Nature, and Oscillator Strengths (*f*) for Each Transition of 7

isomer	band eV (nm)	state	E_{CASPT2}^{Vacuum} eV (nm)	E_{CASPT2}^{PCM} eV (nm)	transition	*f*	relative *f*
E	3.72 (333)	S_1	3.72 (333)	3.69 (336)	(π,π*)	0.4982	0.5609
		S_2	4.64 (267)	4.65 (266)	(π,π*)	0.0009	0.0010
		S_3	4.78 (259)	4.86 (255)	(n,π*)	0.0006	0.0007
		S_4	5.81 (213)	5.75 (215)	$(\pi,\pi^*)^2$, (π,π*)	0.3885	0.4374
Z	3.83 (324)	S_1	3.59 (345)	3.56 (347)	(π,π*)	0.4910	0.5342
		S_2	4.53 (274)	4.54 (273)	(π,π*)	0.0209	0.0227
		S_3	4.74 (262)	4.84 (256)	(n,π*)	0.0078	0.0085
		S_4	6.00 (207)	5.94 (209)	$(\pi,\pi^*)^2$, (π,π*)	0.3995	0.4346

Finally, the photochemistry of the thermally stable *E* isomer was studied as detailed below. Per our calculations, after excitation to the optically bright state S_1 from the Franck–Condon structure, the system relaxes along the stretching coordinate in a first step, leading to bond length alternation of the single and double bonds (d1 from 1.347 to 1.432 Å and d2 from 1.459 to 1.402 Å, see Figure 10 for d1 and d2 definitions). Following the minimum energy path, the system relaxes on the first excited state rotating along the formal double bond ~90 deg. At this point, the energy gap between S_1 and S_0 is ~20 kcal/mol at the CASPT2 level of theory, and the coupling between both states is large (Figure 11).

Figure 11

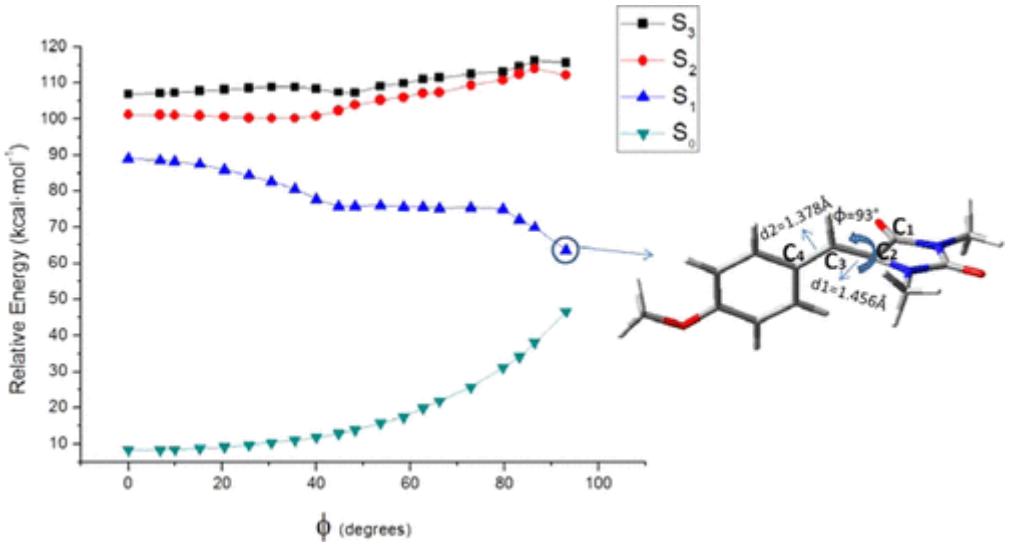

Figure 11. MS-CASPT2 single point energy corrections along the relaxation path on S_1 computed at the CASSCF level of theory as a function of the central double bond torsion coordinate (ϕ) for compound **7**. The structure of the final point is depicted.

From this point, the system can evolve in the ground state after radiative decay, recovering the *E* isomer or completing the photoisomerization reaching the *Z* isomer (Figure 12).

Figure 12

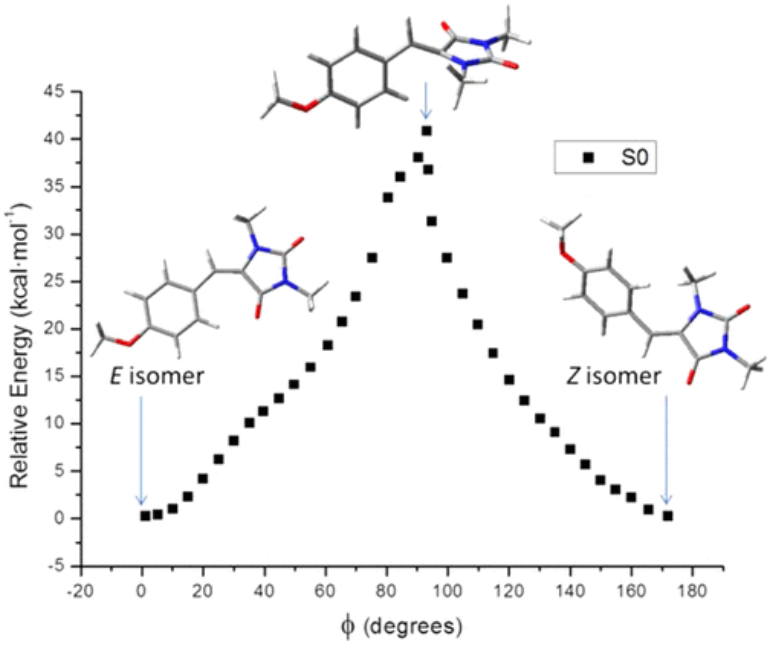

Figure 12. MS-CASPT2 single-point energy corrections along the minimum energy path on S_0 from the S_1 minimum energy structure for **7** computed at the CASSCF level of theory.

Thus, the systems described herein comprise a novel family of efficient photoactive molecular switches as has been computationally verified for one of its derivatives, **7**. Regarding the photophysical properties, the bright state is the first excited state (S_1). Thus, crossings with other excited states that could deactivate the photoisomerization mechanism are avoided. Also, as no minimum was found in the excited state, no emission in the UV–vis region is expected, confirming the experimental findings. Furthermore, these studies also confirm that the solvent effect in the absorption spectra of these systems is not large.

3 Conclusions

The synthesis and detailed photochemical studies of a new family of hydantoin-based molecular photoswitches are presented. Although many applications of molecular switches have appeared in the literature, most employ azobenzenes as the photoactive core. This family has shown impressive potential once incorporated into complex systems, but designing novel uses of switches requires the availability of diverse molecules with a variety of properties. In this contribution, we have established arylidineimidazolidine-2,4-diones as a new family of photoswitches, which are very photostable and can in some cases completely switch between the *on* /*off* state. Their PSS can be controlled by external factors, such as the irradiation source or the filters used. The light energy is used with high efficiency for

photoisomerization as no alternative pathways are available, and they are easy to synthesize and amenable to scale up. Accordingly, mechanistic details obtained from the theoretical calculations allow us to explain the experimental findings. Future studies will focus on modifying these compounds for specific applications. For example, biological applications of these photoswitches currently limited due to absorption maxima in the UV region could be mitigated by affecting the absorption band through substitution to increase the conjugation, including charges in the structure or through sensitized irradiation following already successful strategies for other switches. (1, 2, 23) Also, optical applications could be facilitated by affecting the gap between the absorption bands for the *E* and *Z* isomers and altering the PSS by careful choice of the irradiation wavelength. In conclusion, the arylidineimidazolidine-2,4-dione family consists of a significant extension of the molecular photoswitch concept. Further studies to include these molecules in complex systems are currently underway, along with the design of new systems, including 2-aminoimidazolones and pyrazolones.

4 Experimental Section

General Information

All reactions were carried out in flame-dried glassware. Anhydrous solvents were purchased and used directly. Thin-layer chromatography (TLC) was carried out on precoated glass silica gel plates that were visualized with both ultraviolet light and stained with PMA. ^{1}H and ^{13}C NMR spectra were recorded on a 400 MHz spectrometer. Chemical shifts are reported in ppm with reference to tetramethylsilane [^{1}H NMR: CDCl3 (0.00 δ)] or solvent signals [^{1}H NMR: $CDCl_3$ (7.26 δ), ^{13}C NMR: $CDCl_3$ (77.27 δ)]. Signal patterns are indicated as br (broad peak), s (singlet), d (doublet), t (triplet), q (quartet), and m (multiplet). Infrared spectral data were obtained using a spectrometer with a diamond ATR accessory as the thin film. HRMS (TOF) data was obtained using ESI mode.

Synthesis of Arylideneimidazolidine-2,4-diones

A series of arylideneimidazolidine-2,4-diones were prepared by following one of the two general methods described below.

Method 1

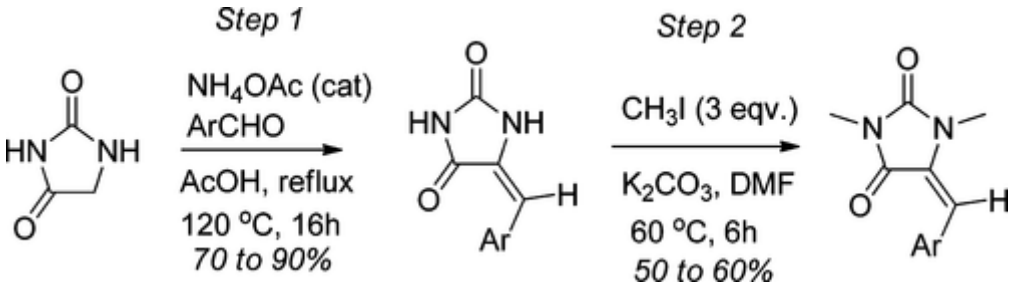

Step 1: A solution of imidazolidine-2,4-dione (2.16 g, 20 mmol) and ammonium acetate (276 mg, 3.6 mmol) in acetic acid (5 mL) was added to aldehyde (20 mmol), and the resulting mixture was stirred at 120 °C for 16 h. After cooling, the reaction mixture was concentrated in vacuum and purified by column chromatography on

silica gel with EtOAc/hexane to afford the 5-arylideneimidazolidine-2,4-diones (with yields ranging from 70 to 90%).

Step 2: To a solution of 5-arylideneimidazolidine-2,4-dione (20 mmol, 2.0 equiv) in dry DMF (50 mL) were added K_2CO_3 (8.3 g, 60 mmol, 3.0 equiv) and methyl iodide (8.51 g, 60 mmol, 3 equiv). The resulting mixture was stirred for 12 h at 60 °C. The reaction was quenched by the addition of water. The resulting mixture was diluted with EtOAc (250 mL) and washed with water (50 mL x 3) and brine (100 mL). The organic layer was dried over anhydrous Na_2SO_4, filtered, and concentrated. The resulting crude residue was purified by column chromatography on silica gel to give 5-arylidine 1,3-dimethylimidazolidine-2,4-diones in 50 to 60% yields.

Method 2

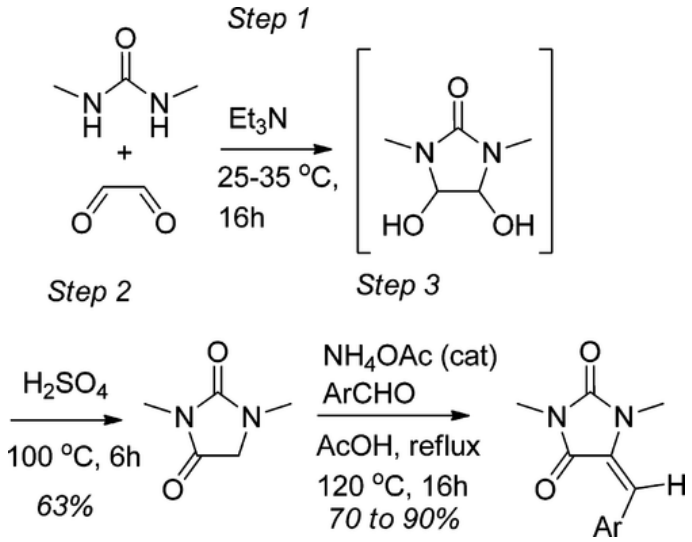

Step 1: A 1000 mL glass round-bottom flask equipped with a stirrer, thermometer, and addition funnel was charged with 290 g (2.0 mol) of 40 wt % aqueous glyoxal solution and triethylamine (pH of the reaction mixture represented 9). Then, while maintaining the liquid temperature at 25–35 °C, a solution 1,3-dimethylurea (176 g, 2.0 mol in 176 mL of water) was gradually added to the mixture. After addition was completed, the mixture was allowed to stir at the same temperature for 3 h. Completion of the reaction was monitored by TLC, after which the solvent was removed under reduced pressure on rotavap to obtain 297 g of crude 4,5-dihydroxy-1,3-dimethyl-2-imidazolidinone qas a colorless oil, which was taken further for step 2 without further purification.

Step 2: A 2000 mL glass round-bottom flask equipped with a stirrer, thermometer, and reflux condenser was loaded with 297 g of crude 4,5-dihydroxy-1,3-dimethyl-2-imidazolidinone prepared from the previous step, H_2O (600 mL), and 98% sulfuric acid (54 g, 0.54 mol), and the resulting mixture was stirred for 6 h at 95–100 °C. After completion of the reaction, the reaction mixture was cooled in an ice bath, and 90 g of sodium bicarbonate was added slowly. The crude residue was diluted with EtOAc/H_2O (500 mL/200 mL). The aqueous layer was separated and extracted with EtOAc (3 × 100 mL). The organic layers were combined and washed with brine (200 mL), dried over anhydrous Na_2SO_4, filtered, and concentrated. The crude residue was purified by column chromatography on silica gel with EtOAc/hexane (20/80 to

35/65) to obtain 1,3-dimethylimidazolidin-2,4-dione as a colorless oil (161 g, 63% yield for two steps).

^{1}H NMR (400 MHz): 3.76 (2H, s), 2.87 (3H, s), 2.87 (3H, s). ^{13}C NMR (100 MHz): 170.0, 157.0, 51.6, 29.5, 24.7. IR: 3444, 2949, 2358, 1760, 1699, 1493, 1419, 1388, 1272, 1248, 1110, 1077, 1005, 756, 599. HR-MS (ESI): calcd for $C_5H_9N_2O_2$ [M + H]$^+$, 129.0664; found, 129.0689.

Step 3: A solution of 1,3-dimethylimidazolidin-2,4-dione (2.56 g, 20 mmol) and ammonium acetate (276 mg, 3.6 mmol) in acetic acid (5 mL) was added to aldehyde (20 mmol), and the resulting mixture was stirred at 115 °C for 16 h. After cooling, the mixture was concentrated in vacuum and purified either by recrystallization or by column chromatography on silica gel with EtOAc/hexane to afford the 5-arylideneimidazolidine-2,4-diones (with yields ranging from 70 to 90%). Spectral data for various (*E*)-5-Arylidene-1,3-dimethylimidazolidine-2,4-diones obtained via the above methods are given below.

(*E*)-5-(Benzylidene)imidazolidine-2,4-dione (*E*-1)

Yield = 2.63 g, 70%. ^{1}H NMR (300 MHz, DMSO-*d*^{6}): δ 7.61 (d, *J* = 7.5 Hz, 2H), 7.40 (t, *J* = 7.4 Hz, 2H), 7.35–7.29 (m, 1H), 6.41 (s, 1H). ^{13}C NMR (300 MHz, DMSO): δ 165.6 (s), 155.7 (s), 133.0 (s), 129.4 (s), 128.8 (s), 128.4 (s), 128.0 (s), 108.3 (s). UV–vis (CH_2Cl_2/MeOH): λ (nm) = 316 (ε = 20471 M^{-1} cm^{-1}), 331 (ε = 16123 M^{-1} cm^{-1}). EM-ES(+): calcd for $C_{10}H_8N_2O_2$ [M + H]$^+$, 189.0664; found, 189.0671. Observations: white solid.

(*Z*)-5-(Benzylidene)imidazolidine-2,4-dione (*Z*-1)

^{1}H NMR (300 MHz, DMSO-*d*^{6})): δ 7.89 (d, *J* = 7.3 Hz, 2H), 7.38–7.28 (m, 3H), 6.32 (s, 1H). ^{13}C NMR (300 MHz, $CDCl_3$): δ 163.6 (s), 153.9 (s), 133.1 (s), 129.9 (s), 128.1 (m), 115.6 (s). UV–vis (CH_2Cl_2/MeOH): λ (nm) = 330 (ε = 13309 M^{-1} cm^{-1}). EM-ES(+): calcd for $C_{10}H_8N_2O_2$ [M + H]$^+$, 189.0664; found, 189.0671. Observations: white solid.

(*E*)-5-(4-Nitrobenzylidene)imidazolidine-2,4-dione (*E*-2)

Yield = 3.63 g, 78%. ^{1}H NMR (400 MHz, DMSO-*d*^{6}): δ 8.19 (d, *J* = 8.4 Hz, 2H), 7.84 (d, *J* = 8.6 Hz, 2H), 6.49 (s, 1H). ^{13}C NMR (100 MHz, DMSO-*d*^{6}): δ 165.3 (s), 155.8 (s), 146.2 (s), 140.0 (s), 130.9 (s), 130.1 (s), 123.7 (s), 105.1 (s). UV–vis (CH_2Cl_2/MeOH (1:1)): λ (nm) = 236 (ε = 8188 M^{-1} cm^{-1}), 353 (ε = 15854 M^{-1} cm^{-1}). EM-ES(+): calcd for $C_{10}H_8N_3O_4$ [M + H]$^+$, 234.0515; found, 234.0515. Observations: brown solid.

(*E*)-5-(2-Hydroxybenzylidene)imidazolidine-2,4-dione (*E*-3)

Yield = 3.06 g, 75%. ^{1}H NMR (400 MHz, DMSO-*d*^{6}): δ 7.53 (d, *J* = 7.7 Hz, 1H), 7.15 (t, *J* = 7.9 Hz, 1H), 6.90–6.77 (m, 2H), 6.67 (s, 1H). ^{13}C NMR (100 MHz, DMSO-*d*^{6}): δ 165.7 (s), 156.0 (s), 155.5 (s), 130.0 (s), 129.5 (s), 127.2 (s), 120.1 (s), 119.4 (s), 115.6 (s), 104.0 (s). UV–vis (CH_2Cl_2/MeOH (1:1)): λ (nm) = 235 (ε = 9800 M^{-1} cm^{-1}), 312 (ε = 13200 M^{-1} cm^{-1}), 340 (ε = 15200 M^{-1} cm^{-1}). EM-ES(+): calcd for $C_{10}H_8N_2O_3$ [M + H]$^+$, 205.0613; found, 205.0615. Observations: white solid.

(*E*)-5-((1*H*-Indol-3-yl)methylene)imidazolidine-2,4-dione (*E*-4)

Yield = 3.35 g, 74%. ^{1}H NMR(400 MHz, DMSO-d^6): δ 8.13 (s, 1H), 7.75 (d, J = 7.7 Hz, 1H), 7.42 (d, J = 7.7 Hz, 1H), 7.21–7.09 (m, 2H), 6.75 (s, 1H). ^{13}C NMR (100 MHz, DMSO): δ 165.7 (s), 155.7 (s), 136.0 (s), 127.0 (s), 126.8(s), 123.8 (s), 122.6 (s), 120.4 (s), 118.2 (s), 112.1 (s), 108.6 (s), 102.1 (s). UV–vis (CH_2Cl_2/MeOH (1:1)): λ (nm) = 275 (ε = 3602 M^{-1} cm^{-1}), 367 (ε = 11835 M^{-1} cm^{-1}). EM-ES(+): calcd for $C_{12}H_9N_3O_2$ $[M+H]^+$, 228. 0773; found, 228.0779. Observations: orange solid.

(*E*)-5-(3,5-Dibromo-4-methoxybenzylidene)imidazolidine-2,4-dione (*E*-5)

Yield = 5.71 g, 77%. ^{1}H NMR (300 MHz, DMSO-d^6): δ 8.09 (s, 2H), 5.59 (s, 1H), 3.76 (s, 3H). ^{13}C NMR (100 MHz, DMSO-d^6): δ 165.4 (s), 155.9 (s), 152.9 (s), 133.0 (s), 132.4 (s), 129.3 (s), 117.9 (s), 104.6 (s), 60.5 (s). UV–vis (CH_2Cl_2/MeOH (1:1)): λ (nm) = 321 (ε = 22605 M^{-1} cm^{-1}). EM-ES(+): calcd for $C_{11}H_8Br_2N_2O_3$ $[M+H]^+$, 374.8980; found, 374.8974. Observations: brown solid.

(*Z*)-5-(3,5-Dibromo-4-methoxybenzylidene)imidazolidine-2,4-dione (*Z*-5)

^{1}H NMR (400 MHz, DMSO-d^6): δ 7.91 (s, 2H), 6.33 (s, 1H), 3.81 (s, 3H). ^{13}C NMR (100 MHz, DMSO-d^6): δ 165.20 (s), 155.7 (s), 153.0 (s), 133.0 (s), 132.1 (s) 129.1 (s), 117.9 (s), 104.5 (s), 60.5 (s). UV–vis (CH_2Cl_2/MeOH (1:1)): λ (nm) = 328 (ε = 14942 M^{-1} cm^{-1}), 342 (ε = 5747 M^{-1} cm^{-1}). EM-ES(+): calcd for $C_{11}H_8Br_2N_2O_3$ $[M+H]^+$, 374.8980; found, 374.8974. Observations: brown solid.

(*E*)-5-(Benzylidene)-1,3-dimethylimidazolidine-2,4-dione (*E*-6)

Yield = 3.51 g, 81%. ^{1}H NMR (300 MHz, $CDCl_3$): δ 7.41–7.28 (m, 5H), 6.95 (s, 1H), 3.14 (s, 3H), 2.95 (s, 3H). ^{13}C NMR (300 MHz, $CDCl_3$): δ 163.7 (s), 155.8 (s), 132.6 (s), 129.6 (s), 129.4 (s), 128.3 (s), 128.2 (s), 112.2 (s), 30.5 (s), 24.9 (s). UV–vis ($CHCl_3$): λ (nm) = 240 (ε = 7904 M^{-1} cm^{-1}), 309 (ε = 12316 M^{-1} cm^{-1}). EM-ES(+): calcd for $C_{12}H_{12}N_2O_2$ $[M+H]^+$, 217.0977; found, 217.0972. Observations: yellow oil.

(*E*)-5-(4-Methoxybenzylidene)-1,3-dimethylimidazolidine-2,4-dione (*E*-7)

Yield = 3.95 g, 80%. ^{1}H NMR (400 MHz, CD_3CN): δ 7.96 (d, J = 8.9 Hz, 2H), 6.92 (d, J = 8.9 Hz, 2H), 6.28 (s, 1H), 3.81 (s, 3H), 3.12 (s, 3H), 2.98 (s, 3H). ^{13}C NMR (100 MHz, CD_3CN): δ 163.1 (s), 161.1 (s), 154.6 (s), 133.0 (s), 129.1 (s), 126.8 (s), 117.4 (s), 114.5 (s), 56.0 (s), 26.8 (s), 24.9 (s). UV–vis ($CHCl_3$): λ (nm) = 333 (ε = 16346 M^{-1} cm^{-1}), 243 (ε = 10115 M^{-1} cm^{-1}). ES-MS(+): calcd for $C_{13}H_{14}N_2O_3$ $[M+H]^+$, 247.1083; found, 247.1065. Observations: yellow solid. CCDC 922962 contains the crystallographic data for this compound.

(*Z*)-5-(4-Methoxybenzylidene)-1,3-dimethylimidazolidine-2,4-dione (*Z*-7)

^{1}H NMR (400 MHz, $CDCl_3$): δ 7.24 (d, J = 8.7 Hz, 2H), 6.93 (s, 1H), 6.90 (d, J = 3.8 Hz, 2H), 3.84 (s, 3H), 3.13 (s, 3H), 3.00 (s, 3H). ^{13}C NMR (100 MHz, $CDCl_3$): δ 164.0 (s), 159.9 (s), 156.2 (s), 131.1 (s), 129.0 (s), 124.9 (s), 113.9 (s), 112.7 (s), 55.4 (s), 30.6 (s), 25.1 (s). UV–vis ($CHCl_3$): λ (nm) = 325 (ε = 14808 M^{-1} cm^{-1}). ES-MS(+): calcd for $C_{13}H_{14}N_2O_3$ $[M+H]^+$, 247.1083; found, 247.1065. Observations: yellow solid.

(*E*)-5-(4-Nitrobenzylidene)-1,3-dimethylimidazolidine-2,4-dione (*E*-8)

Yield = 4.71g, 90%. ^{1}H NMR (300 MHz, $CDCl_3$): δ 8.27 (d, *J* = 8.4 Hz, 2H), 7.47 (d, *J* = 8.5 Hz, 2H), 6.89 (s, 1H), 3.17 (s, 3H), 2.96 (s, 3H). ^{13}C NMR (400 MHz, $CDCl_3$): δ 163.3 (s), 155.7 (s), 147.5 (s), 139.8 (s), 131.7 (s), 130.4 (s), 123.6 (s), 108.7 (s), 30.7 (s), 25.4 (s). UV–vis ($CHCl_3$): λ (nm) = 339 (ε = 11816 M^{-1} cm^{-1}). EM-ES(+): calcd for $C_{12}H_{11}N_3O_4$ $[M+H]^+$, 262.0828; found, 262.0822. Observations: orange solid.

(*E*)-5-(2-Methoxybenzylidene)-1,3-dimethylimidazolidine-2,4-dione (*E*-9)

Yield = 3.91 g, 79%. ^{1}H NMR (300 MHz, $CDCl_3$): δ 7.34 (t, *J* = 7.4 Hz, 1H), 7.16 (d, *J* = 7.4 Hz, 1H), 7.02–6.88 (m, 3H), 3.85 (s, 3H), 3.13 (s, 3H), 2.94 (s, 3H). ^{13}C NMR (300 MHz, $CDCl_3$): δ 163.6 (s), 157.6 (s), 155.8 (s), 130.7 (s), 130.0 (s), 129.9 (s), 121.5 (s), 119.9 (s), 110.4 (s), 108.8 (s), 55.4 (s), 29.8 (s), 4.9 (s). UV–vis ($CHCl_3$): λ (nm) = 242 (ε = 10870 M^{-1} cm^{-1}), 326 (ε = 12077 M^{-1} cm^{-1}). EM-ES(+): calcd for $C_{13}H_{14}N_2O_3$ $[M+H]^+$, 247.1083; found, 247.1077. Observations: brown solid.

(*E*)-5-((1-Methyl-indol-3-yl)methylene)-1,3-dimethylimidazolidine-2,4-dione (*E*-10)

Yield = 4.42 g, 82%. ^{1}H NMR (300 MHz, $CDCl_3$): δ 7.68 (d, *J* = 8.0 Hz, 1H), 7.34 (t, *J* = 8.3 Hz, 2H), 7.24–7.19 (m, 1H), 7.15 (s, 1H), 7.10 (s, 1H), 3.85 (s, 3H), 3.17 (s, 3H), 3.15 (s, 3H). ^{13}C NMR (400 MHz, $CDCl_3$): δ 164.2 (s), 156.4 (s), 136.8 (s), 129.8 (s), 128.4 (s), 127.5 (s), 123.0 (s), 120.8 (s), 119.7 (s), 109.93 (m), 107.7 (s), 106.0 (s), 33.3 (d, *J* = 15.0 Hz), 30.2 (s), 25.1 (s). UV–vis ($CHCl_3$): λ (nm) = 373 (ε = 13610 M^{-1} cm^{-1}). EM-ES(+): calcd for $C_{15}H_{15}N_3O_2$ $[M+H]^+$, 270.1243; found, 270.1242. Observations: brown solid.

(*E*)-5-(3,5-Dibromo-4-methoxybenzylidene)-1,3-dimethylimidazolidine-2,4-dione (*E*-11)

Yield = 6.75 g, 84%. ^{1}H NMR (400 MHz, $CDCl_3$): δ 7.44 (s, 2H), 6.72 (s, 1H), 3.92 (s, 3H), 3.14 (s, 3H), 3.00 (s, 3H). ^{13}C NMR (300 MHz, $CDCl_3$): δ 163.4 (s), 155.8 (s), 154.3 (s), 133.5 (s), 131.4 (s), 131.0 (s), 118.2 (s), 108.2 (s), 61.0 (s), 30.8 (s), 25.3 (s). UV–vis ($CHCl_3$): λ (nm) = 316 (ε = 8710 M^{-1} cm^{-1}). EM-ES(+): calcd for $C_{13}H_{12}Br_2N_2O_3$ $[M+H]^+$, 402.9293; found, 402.9282. Observations: yellow solid.

Typical Procedure of Irradiation

The solutions of photoswitches **1**–**5** in DMSO (0.01 M) and **7**–**11** in $CDCl_3$ (0.01 M) were prepared and irradiated in separate NMR tubes using a 400 W medium-pressure Hg lamp until the PSS was reached. The reaction was followed by ^{1}H NMR spectroscopy. A similar procedure was followed with a light source centered at 350 nm. The solutions were placed in a merry-go-round appliance in a photoreactor and irradiated using lamps with an emission wavelength centered at 350 nm (14 lamps × 8 W/lamps) until the PSS was reached.

Selective Irradiation of *Z* and *E* Isomers of 7

The two isomers (*Z* and *E*) of compound **7** were irradiated separately with monochromatic light at irradiation wavelengths of 300, 330, and 375 nm. All experiments were carried out under the same conditions with the same intensity of

monochromatic light. Solutions (5.36×10^{-5} M) were prepared in dry acetonitrile. Three milliliters of these solutions were irradiated at the selected wavelengths in a quartz cuvette (1.0 cm path length) using a monochromator until the PSS was reached. The photochemical reaction was followed by GC/MS.

Isomerization Quantum Yield

The isomerization quantum yield (photoswitch **4** or **7**) was calculated following the procedure described in the literature using *trans*-azobenzene as an actinometer. First, a solution of *trans*-azobenzene in acetonitrile was prepared. The absorbance of this solution at 358 nm was set to 1. Then, the actinometer solution was irradiated in a quartz cuvette at 334 nm using a monochromator. After a short period of time, the change in absorbance at 358 nm was ~0.02. A solution in acetonitrile (for **7**) or CH_2Cl_2/MeOH (1:1) (for **4**) was prepared. The absorbance at 334 nm was adjusted to match the value of the actinometer. This solution was irradiated at 334 nm until a conversion of 20% was reached. The isomerization process was followed by GC/MS. The number of photons absorbed by the sample was calculated using the following formula $\mathrm{Ep\ (mol\ of\ photons \times cm^{-2} \times s^{-1}) = F(\lambda) \times \Delta A(358nm)/t(s)}$ where ΔA(358 nm) is the change in the absorbance at 358 nm of the *trans*-azobenzene solution when irradiated at 334 nm, and t(s) is the irradiation time responsible for that change. The F factor, which depends on the wavelength, has a value of 3.6×10^{-6} einstein cm^{-2} at 334 nm. Thus, the number of photons absorbed corresponds to Ep multiplied by the irradiation time (in seconds). The photochemical isomer formed after irradiation is quantified by GC/MS. The value for the isomerization quantum yield is obtained from the following equation $\phi = \dfrac{\text{number of formed or destroyed molecules}}{\text{number of photons absorbed by the system}}$

Finally, the actinometer solution was measured again to ensure that the light intensity is constant. All solutions were kept in the dark during the entire experiment.

(1) Balzani, V.; Credi, A.; Venturi, M. Molecular Devices and Machines: Concepts and Perspectives for the Nanoworld; Wiley-VCH Verlag: Weinheim, Germany, 2008.
(2) Molecular Switches, 2nd ed.; Feringa, B. L., Browne, W. R., Eds.; Wiley-VCH: Weinheim, Germany, 2011.
(3) Bushuyev, O. S.; Tomberg, A.; Fris˘c˘ic´, T.; Barrett, C. J. J. Am. Chem. Soc. 2013, 135, 12556.
(4) Ritterson, R. S.; Kuchenbecker, K. M.; Michalik, M.; Kortemme, T. J. Am. Chem. Soc. 2013, 135, 12516.
(5) Szyman´ski, W.; Beierle, J. M.; Kistemaker, H. A. V.; Velema, W. A.; Feringa, B. L. Chem. Rev. 2013, 113, 6114.
(6) Bogdavov, A.; Bobrovsky, A.; Ryabchun, A.; Vorobiev, A. Phys. Rev. E 2012, 85, 011704.
(7) Mitchell, R. H. Eur. J. Org. Chem. 1999, 1999, 2695.
(8) Muratsugu, S.; Kume, S.; Nishihara, H. J. Am. Chem. Soc. 2008, 130, 7204.
(9) Roldan, D.; Kaliginedi, V.; Cobo, S.; Kolivoska, V.; Bucher, C.; Hong, W.; Royal, G.; Wandlowski, T. J. Am. Chem. Soc. 2013, 135, 5974.
(10) Vila`, N.; Royal, G.; Loiseau, F.; Deronzier, A. Inorg. Chem. 2011, 50, 10581.
(11) Irie, M. Chem. Rev. 2000, 100, 1685.
(12) Irie, M.; Fukaminato, T.; Matsuda, K.; Kobatake, S. Chem. Rev. 2014, 114, 12174.
(13) Tian, H.; Yang, S. Chem. Soc. Rev. 2004, 33, 85.
(14) Ivashenko, O.; van Herpt, J. T.; Feringa, B. L.; Rudolf, P.; Browne, W. R. Langmuir 2013, 29, 4290.
(15) Koc¸er, A.; Walko, M.; Meijberg, W.; Feringa, B. L. Science 2005, 309, 755.
(16) Kohl-Landgraf, J.; Braun, M.; O¨zc¸oban, C.; Gonc¸alves, D. P. N.; Heckel, A.; Wachtveitl, J. J. Am. Chem. Soc. 2012, 134, 14070.
(17) Lukyanov, B. S.; Lukyanova, M. B. Chem. Heterocycl. Compd. 2005, 41, 281.

(18) Beharry, A. A.; Woolley, G. A. Chem. Soc. Rev. 2011, 40, 4422.
(19) Samanta, S.; Woolley, G. A. Chembiochem 2011, 12, 1712.
(20) Zarwell, S.; Ruck-Braun, K. Tetrahedron Lett. 2008, 49, 4020.
(21) Feringa, B. L. J. Org. Chem. 2007, 72, 6635.
(22) London, G.; Chen, K.-Y.; Carroll, G. T.; Feringa, B. L. Chem.Eur. J. 2013, 19, 10690.
(23) Garcia-Iriepa, C.; Marazzi, M.; Frutos, L. M.; Sampedro, D. RSC Adv. 2013, 3, 6241.
(24) Blanco-Lomas, M.; Campos, P. J.; Sampedro, D. Eur. J. Org. Chem. 2012, 2012, 6328.
(25) Blanco-Lomas, M.; Samanta, S.; Campos, P. J.; Woolley, G. A.; Sampedro, D. J. Am. Chem. Soc. 2012, 134, 6960.
(26) Andruniow, T.; Fantacci, S.; De Angelis, F.; Ferre, N.; Olivucci, M. Angew. Chem., Int. Ed. 2005, 44, 6077.
(27) Melloni, A.; Rossi Paccani, R.; Donati, D.; Zanirato, V.; Sinicropi, A.; Parisi, M. L.; Martin, E.; Ryazantsev, M.; Ding, W. J.; Frutos, L. M.; Basosi, R.; Fusi, S.; Latterini, L.; Ferre´, N.; Olivucci, M. J. Am. Chem. Soc. 2010, 132, 9310.
(28) Rivado-Casas, L.; Sampedro, D.; Campos, P. J.; Fusi, S.; Zanirato, V.; Olivucci, M. J. Org. Chem. 2009, 74, 4666.
(29) Sinicropi, A.; Martin, E.; Ryasantsev, M.; Helbing, J.; Briand, J.; Sharma, D.; Le´onard, J.; Haacke, S.; Canizzo, A.; Chergui, M.; Zanirato, V.; Fusi, S.; Santoro, F.; Basosi, R.; Ferre´, N.; Olivucci, M. Proc. Natl. Acad. Sci. U.S.A. 2008, 105, 17642.
(30) Blanco-Lomas, M.; Funes-Ardoiz, I.; Campos, P. J.; Sampedro, D. Eur. J. Org. Chem. 2013, 2013, 6611.
(31) Funes-Ardoiz, I.; Blanco-Lomas, M.; Campos, P. J.; Sampedro, D. Tetrahedron 2013, 69, 9766.
(32) Cordes, T.; Elsner, C.; Herzog, T. T.; Hoppmann, C.; Schadendorf, T.; Summerer, W.; Ru¨ck-Braun, K.; Zinth, W. Chem. Phys. 2009, 358, 103.
(33) Cordes, T.; Schadendorf, T.; Ru¨ck-Braun, K.; Zinth, W. Chem. Phys. Lett. 2008, 455, 197.
(34) Cordes, T.; Weinrich, D.; Kempa, S.; Riesselmann, K.; Herre, S.; Hoppmann, C.; Ru¨ck-Braun, K.; Zinth, W. Chem. Phys. Lett. 2006, 428, 167.
(35) Regner, N.; Herzog, T. T.; Haiser, K.; Hoppmann, C.; Beyermann, M.; Sauermann, J.; Engelhard, M.; Cordes, T.; Ru¨ck- Braun, K.; Zinth, W. J. Phys. Chem. B 2012, 116, 4181.
(36) Schadendorf, T.; Hoppmann, C.; Ru¨ck-Braun, K. Tetrahedron Lett. 2007, 48, 9044.
(37) Steinle, W.; Ru¨ck-Braun, K. Org. Lett. 2002, 5, 141.
(38) Maerz, B.; Wiedbrauk, S.; Oesterling, S.; Samoylova, E.; Nenov, A.; Mayer, P.; de Vivie-Riedle, R.; Zinth, W.; Dube, H. Chem.Eur. J. 2014, 20, 13984.
(39) García-Iriepa, C.; Marazzi, M.; Zapata, F.; Valentini, A.; Sampedro, D.; Frutos, L. M. J. Phys. Chem. Lett. 2013, 4, 1389.
(40) Ruhemann, S.; Cunnington, A. J. Chem. Soc. 1899, 75, 945.
(41) Wheeler, H. L.; Hoffman, C. Am. Chem. J. 1911, 45, 368.
(42) Anticancer: (a) Kaminskyy, D. V.; Lesyk, R. B. Biopolym. Cell 2010, 26, 136 − 145. (b) El-Deeb, I. M.; Bayoumi, S. M.; El-Sherbeny, M. A. Eur. J. Med. Chem. 2010, 45, 2516 − 2530. Antibiotic: (c) Handzlik, J.; Szyman´ska, E.; Alibert, S.; Chevalier, J.; Otrębska, E.; Pękala, E.; Page`s, J.-M.; Kiec´-Kononowicz, K. Bioorg. Med. Chem. 2013, 21, 135 − 145. (d) Handzlik, J.; Matys, A.; Kiec´-Kononowicz, K. Antibiotics 2013, 2, 28 − 45. Antagonistic: (e) Handzlik, J.; Szyman´ska, E.; Wo´jcik, R. Bioorg. Med. Chem. 2012, 20, 4245 − 4257.
(43) Takano, S.; Kobayashi, T. J. Soc. Cosmet. Chem. Jpn. 1993, 26, 262.
(44) Blanco-Lomas, M.; Campos, P. J.; Sampedro, D. Org. Lett. 2012, 14, 4334.
(45) Tan, S. F.; Ang, K. P.; How, G. F. J. Phys. Org. Chem. 1990, 3, 559.
(46) Tan, S. F.; Ang, K. P.; How, G. F. J. Phys. Org. Chem. 1991, 707.
(47) Ware, E. Chem. Rev. 1950, 46, 403.
(48) Johnson, T. B.; Nicolet, B. H. J. Am. Chem. Soc. 1912, 34, 1048.
(49) In the setup used, the excitation spectrum was taken by moving the primary monochromator of the spectrofluorometer while keeping the reading wavelength of the secondary one fixed. As these compounds feature very weak intensities, the slit in the secondary monochromator has to be wide open to read the emission pattern. Therefore, the emission spectrum is obtained only for the registered absorption. The excitation spectrum shows the range of wavelengths that provide the emission spectrum. If this compound would have another emission band corresponding to a different excited state, we would get a different excitation band. Therefore, the excitation spectrum may be the same as the absorption spectrum. In contrast, the absorption spectrum must contain the excitation spectra.
(50) Kuhn, H. J.; Braslavsky, S. E.; Schmidt, R. Pure Appl. Chem. 2004, 76, 2105.

(51) Izquierdo-Serra, M.; Gasco´n-Moya, M.; Hirtz, J. J.; Pittolo, S.; Poskanzer, K. E.; Ferrer, E`.; Alibe´s, R.; Busque´, F.; Yuste, R.; Hernando, J.; Gorostiza, P. J. Am. Chem. Soc. 2014, 136, 8693.
(52) Computational Photochemistry; Olivucci, M., Ed.; Elsevier: Amsterdam, 2005.
(53) Sampedro, D. In Photochemistry: UV/VIS Spectroscopy, Photochemical Reactions and Photosynthesis; Maes, K. J., Willems, J. M., Eds.; Nova Science Publishers: Hauppauge, New York, 2011.